Applied Magnetic Resonance (2019) 50:809–818
https://doi.org/10.1007/s00723-018-1085-z

Applied
Magnetic Resonance

ORIGINAL PAPER

Magnetic Phase Transition and Exchange Bias in $Ni_{45}Co_5Mn_{35.5}In_{14.5}$ Heusler Alloy

Łukasz Dubiel[1] · Antoni Żywczak[2] · Wojciech Maziarz[3] · Ireneusz Stefaniuk[4] · Andrzej Wal[4]

Received: 28 June 2018 / Revised: 3 October 2018 / Published online: 26 October 2018

Abstract

Magnetic properties and exchange bias of $Ni_{45}Co_5Mn_{35.5}In_{14.5}$ ribbons were investigated by vibrating sample magnetometry (VSM) and electron magnetic resonance (EMR). Curie temperatures determined by using VSM and EMR methods are equal to 374 K and 377 K, respectively. Additionally, the EMR measurements revealed the existence of a weak ferromagnetic resonance (FMR) line in the paramagnetic region. The upward deviation of the integral intensity from Curie–Weis low below temperature T^* and above T_C confirms the existence of ferromagnetic phase in this temperature region. Below T_C, the integral intensity does not saturate, which can suggest the coexistence of different magnetic phases at low temperature range. Additional confirmation on the coexistence of magnetic phases in the sample are asymmetric hysteresis loops associated with the spontaneous exchange bias effect. The dependence of EMR signal on cyclic repetition of measurement is also discussed.

1 Introduction

Ni-Mn-In and Co-doped alloys have received much attention in recent years, due to their magnetic and structural properties [1]. The highest interest in Ni-Mn based Heusler alloys has focused first on gallium alloys. However, off-stoichiometric Ni-Mn-In, in certain composition range, has similar properties to Ni-Mn-Ga. Additionally, indium is significantly cheaper than gallium, which makes Ni-Mn-In

✉ Łukasz Dubiel
lukasz.dubiel@ijf.edu.pl

[1] International PhD Studies, Institute of Nuclear Physics Polish Academy of Sciences, Cracow, Poland

[2] Academic Centre for Materials and Nanotechnology, AGH University of Science and Technology, Cracow, Poland

[3] Institute of Metallurgy and Material Science Polish Academy of Sciences, Cracow, Poland

[4] Faculty of Mathematics and Natural Sciences, University of Rzeszow, Rzeszow, Poland

attractive for future practical application [2, 3], but the main problem is its brittleness. The brittleness can be reduced by Co addition. The substitution of Co for Ni in Ni-Mn-In alloys causes the formation of the dispersive secondary γ phase [4, 5], which improves plasticity. However, some method of sample fabrication can reduce this phase [6]. What is more, the Curie temperature T_C and the martensitic transition temperature are shifted to higher and lower temperatures, respectively [7]. However, for some fraction of Co, structural phase transition disappears.

In these groups of materials the unidirectional anisotropy called exchange bias (EB) [8, 9] was observed. The EB behavior is visible as a shift of the magnetic hysteresis loop along the field axis [10]. The EB effect has been observed in a multilayer structure, but has also been reported for Heusler alloys in a polycrystalline form [8] and ribbon shape [6]. In the multilayer samples, the EB effect is related to the interactions between antifferomagnetic (AFM) and ferromagnetic (FM) layers, while in the bulk samples the EB behavior originates from coexisting AFM and FM areas. Reports about such coexistence in alloys type Ni-Mn-X can be found in papers [9, 11]. The theoretical explanation of different kinds of magnetism observed in these materials, i.e., FM and AFM, is based on the RKKY model of interaction between Mn atoms. The sign of the exchange constant in it depends on the distance between these atoms [12]. Owing to the discovery of the exchange bias and the large magnetoresistance, Ni-Mn based Heusler alloys have potential application in different areas: ultrahigh-density recording, giant magnetoresistance, and spin valve [13, 14].

In this paper, we present an investigation of the magnetic behavior of Heusler alloy $Ni_{45}Co_5Mn_{35.5}In_{14.5}$ in ribbon shape. The paper consists of two main sections. In the first section, description of the sample and the experimental apparatus is placed. The second contains discussion of results.

2 Experimental

The alloy with the nominal composition of $Ni_{45}Co_5Mn_{35.5}In_{14.5}$ was prepared by melt-spinning method in ribbon flakes form. This alloy was formed according to the procedure, which was described in [15].

Electron magnetic resonance (EMR) measurements were obtained using the Bruker ELEXYS E580 multifrequency spectrometer equipped with the Bruker liquid N gas flow cryostat with the 41131 VT digital controller. Spectra were registered during the cooling process in the temperature range of 280–410 K in the X-band (9.45 GHz). The cycles dependency was recorded at room temperature and in the 0–0.7 T static magnetic field range.

The magnetization curves were obtained by the LakeShore 7407 vibrating sample magnetometry (VSM). Field-cooled (FC) and field-heated (FH) curves were registered at $\mu_0 H = 0.005$ T in the temperature range of 100-400 K. In addition, hysteresis loops at room temperature were recorded as function of an increasing angle φ (with 15° step) up to 180°, and φ is the angle between the direction of the field and the symmetry axis of a rectangular sample (Fig. 7). In EMR and VSM measurements, the external magnetic field was applied in a plane of the ribbon.

3 Results and Discussion

Figure 1 presents the magnetization curves for the FC and FH process at $\mu_0 H = 0.005$ T obtained by the VSM method. With decreasing temperature, the magnetization increases rapidly. This behavior is related to the second-order magnetic phase transition. It is noteworthy that practically, there is no temperature hysteresis in the magnetisation as a function of temperature, i.e., heating and cooling give the same shape of $M(T)$. This is the second confirmation that this is the second-order phase transition and that alloy does not reveal the martensite phase transition in this range of temperature [15]. The phase transition temperature T_C from paramagnetic to ferromagnetic state was estimated from the minimum of dM/dT vs. T curves (inset on the Fig. 1) and is equal to 374 K.

The EMR spectra of $Ni_{45}Co_5Mn_{35.5}In_{14.5}$ for various temperatures are shown in Fig. 2. The sample has strong EMR signal, so the measurements were made with an attenuation equals 20 dB. With decreasing temperature, the EMR signal increases, broadens and shifts to the low field. The linewidth of the EMR signal, calculated as a peak–peak width, versus temperature is presented in the Fig. 3. At the high temperatures, the main EMR line is asymmetric. This shape is usually attributed to metallic samples and described by the Dyson theory [20]. This main line was well fitted by derivative of Dysonian function [21]:

$$\frac{dP}{dB} = \frac{d}{dB}\left(\frac{\Delta B + \alpha(B - B_r)}{(B - B_r)^2 + \Delta B^2}\right) + \frac{d}{dB}\left(\frac{\Delta B + \alpha(B + B_r)}{(B + B_r)^2 + \Delta B^2}\right), \quad (1)$$

where ΔB is the linewidth, B_r is the resonance field and α is the asymmetry parameter. The result of fitting is presented in Fig. 4. The resonance field of this line

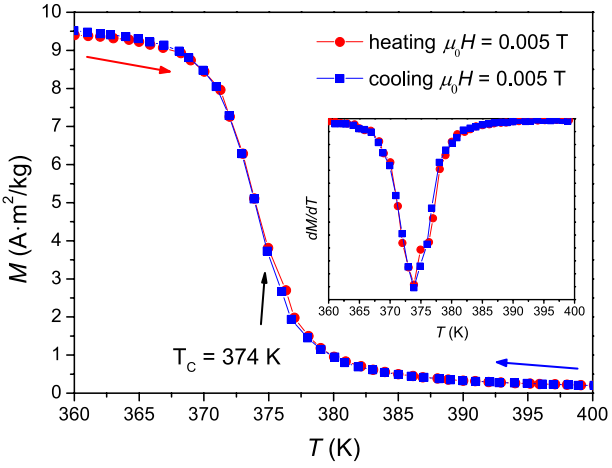

Fig. 1 FC and FH magnetization curves as a function of temperature of the $Ni_{45}Co_5Mn_{35.5}In_{14.5}$ melt-spun ribbon at $\mu_0 H = 0.005$ T. The temperature dependence of dM / dT is shown in the inset

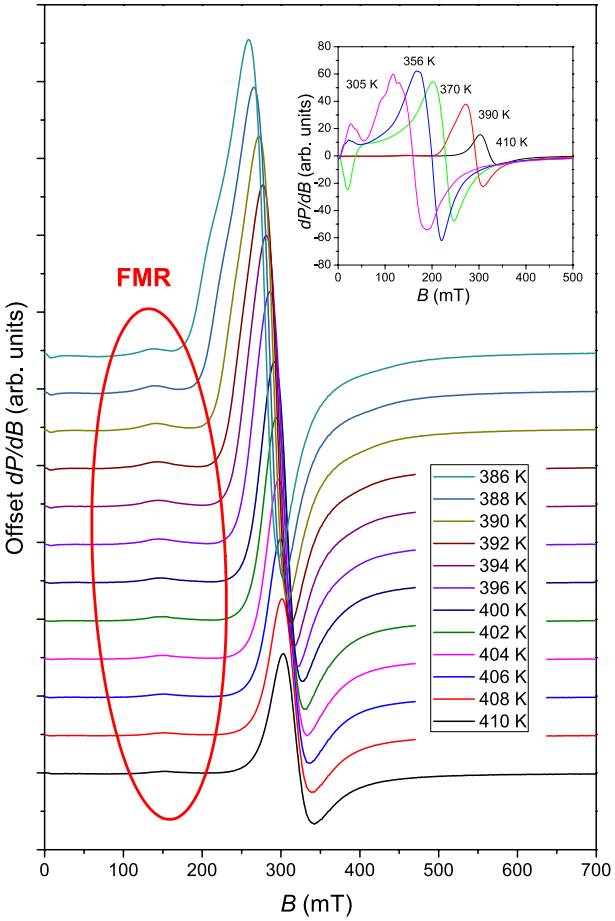

Fig. 2 Samples of EMR spectra of $Ni_{45}Co_5Mn_{35.5}In_{14.5}$ ribbon for various temperatures (high-temperature region). Inset shows the line evolution with decrease in temperature

corresponds to an effective g value close to 2 and has a typical behavior for paramagnetic (PM) phase. However, at the PM region (above T_C), the EMR spectra exhibit a weak signal at the low field region (see Fig. 2). The presence of the extra line at the PM region can give the evidence for the existence of the additional magnetic phase in this material. A similar character of the EMR spectra has been reported by other authors for manganites [16–19], where this phenomena were assigned to Griffiths phase [22], and for amorphous Fe-rich $Fe_{100-x}Zr_x$ alloys [23], where the explanation of the resonance above T_C was based on the model of infinite ferromagnetic matrix and finite spin clusters embedded in, but isolated (in sense of ferromagnetic interaction) from, this infinite cluster. In our case, however, the behavior of the FM signal is a little different from that reported in the above cited papers. Its intensity decreases with increasing temperature, but remains still separated from the PM signal. Additionally, with decreasing temperature two signals merge together below 385 K.

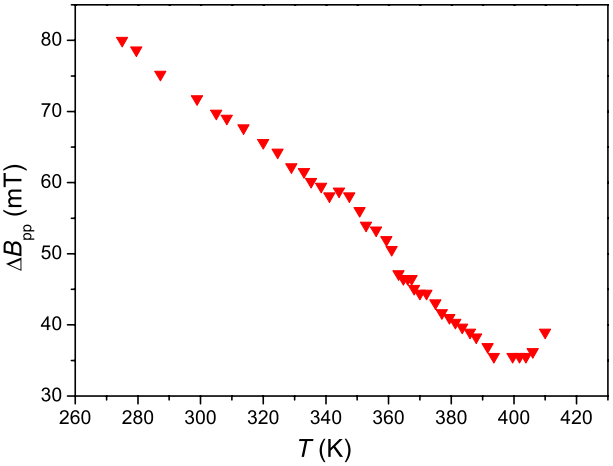

Fig. 3 ΔB_{pp} curve as a function of temperature of the $Ni_{45}Co_5Mn_{35.5}In_{14.5}$ melt-spun ribbon

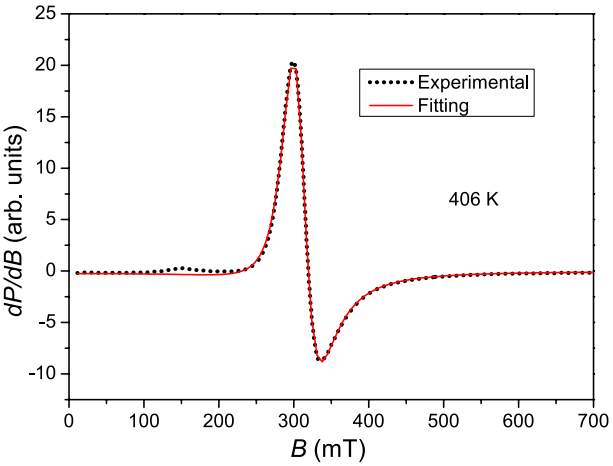

Fig. 4 High-temperature EMR signal obtained for $Ni_{45}Co_5Mn_{35.5}In_{14.5}$. The solid line is the Dysonian fit of the "main" line of EMR signal. The dotted line indicates experimental data

In the low temperature region, the complicated shape of the signal indicates the existence of several resonance lines. This behavior could be related to the structure and different magnetic interactions observed in the $Ni_{45}Co_5Mn_{35.5}In_{14.5}$ sample. The structural properties of such material in ribbon form has been reported in paper [15]. SEM (scanning electron microscope) investigation revealed a two-layered structure. One layer forms columnar grains, whose longest axis is perpendicular to the ribbon surface. In the region near the surface, which was in contact with the wheel during ribbon formation, the small grains are visible (see Fig. 1 in cited above article). TEM (transmission electron microscope) investigation

showed that at room temperature, the main structural phase was austenite in the $L2_1$ phase with some addition of modulated 14M martenisities located at the grain boundaries.

The interaction between Mn atoms at Mn and In position in the investigated alloy in austenite phase is always ferromagnetic [24]. For martensitie, the phase situation is much more complicated. They are several models proposed for the explanation of the properties of this phase in different temperature regions: ferromagnetic and antiferromagnetic interaction, superparamagnetism, superspin glasses, sequence of paramagnetic to ferromagnetic phases (for details see references in cited paper [24]). Based on the above arguments, the detailed explanation of observed EMR signals is difficult and needs further studies.

The temperature dependency of the inverse integral intensity $1/I_{\mathrm{int}}(T)$ (proportional to $1/\chi$) was used to determine Curie temperature (Fig. 5). The determined T_{C} is equal to 377 K and this value is in a good agreement with the value estimated by the VSM method (374 K). The EMR spectra give information about the additional magnetic phase (Fig. 2), which has not been revealed in the VSM measurements. The upward deviation from Curie–Weiss low, visible on Fig. 5 below temperature $T^* = 387$ K (in which deviation appears), suggests that this phase is ferromagnetic [25]. The inset in Fig. 5 shows the integral intensity I_{int} as a function of temperature. With decrease in temperature, I_{int} increases, but not saturates. The VSM method does not give any information about other magnetic phases, and these results indicate that EMR is a very effective technique to probe the local magnetic inhomogeneity.

The hysteresis loops for different orientations of the sample were also determined. The magnetic field was changed in the range $-40 \cdots +40$ kA/m and the direction of it was parallel to the plane, having angle φ with the symmetry axis of the rectangular sample. The direction in plane was chosen since the thickness is much smaller than the width and the length of the specimen, so it is expected that the magnetization vector lies in the plane.

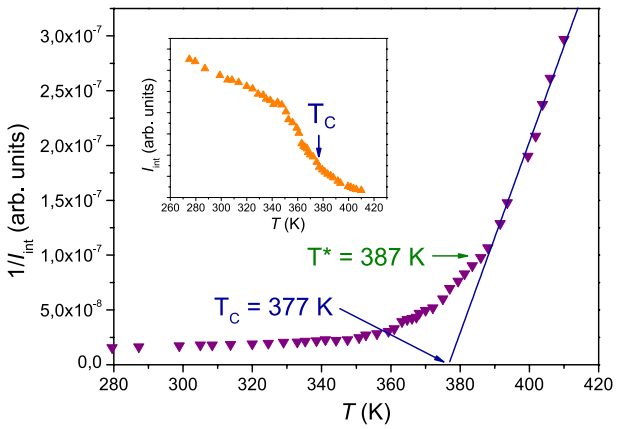

Fig. 5 Inverse integral intensity of EMR signal versus temperature of the $Ni_{45}Co_5Mn_{35.5}In_{14.5}$ ribbon for the cooling process. The inset shows the integral intensity versus temperature

An angular dependence of the curve slope $M(H)$ was observed, which suggests the existence of magnetic anisotropy. Its source could be explained considering the shape of the sample. The calculation of demagnetizing factors for the rectangular prism can be done according to the analytical formula given in the paper [26]. For example, for a cuboid having dimension $a = 2$ mm, $b = 0.1$ mm and $c = 4$mm, where a is the width of the sample, b its thickness and c its length, the values of demagnetizing factors are given by the numbers: $D_a = 0.065$, $D_b = 0.904$ and $D_c = 0.032$. The subscript of D denotes the direction of the axis along which the calculation was done. From these values, one can conclude that the easy axis will be along the direction of the longest side of the rectangle. This is in accordance with the experimental result, for which the greatest increase in the magnetization M for increasing H field is observed, when the direction of the field is parallel to the longest edge of the sample (see Fig. 6). The width of these loops are small, i.e., the coercive field H_c is small, but after limiting the field interval, it can be noted that this width changes with the angle φ (see Fig. 6 part a and c). The largest width occurs along the direction of the easy axis, and the smallest one appears at the angle $\varphi = 90°$.

Despite the fact that the width of the hysteresis is very small, i.e., the loop is narrow, one can observe the shift of its center into the negative field direction (see Fig. 6a). This can suggest the existence of an exchange bias effect. Reports on the occurrence of this phenomenon in NiMnIn-based Heusler alloys can be found. Pathak et al. [27] have reported the EB properties of this material in bulk form, whereas Zhao et al. [6] have described this effect for the ribbon form. The EB was also observed in $Ni_{48}Mn_{39.5}Sn_{9.5}Al_3$ ribbons [28]. The explanation of these phenomena was based on the existence in low temperature of both magnetic phases, i.e., ferromagnetic and antiferromagnetic. For our sample, the value of exchange bias field is very small $H_e \approx 0.1$ kA/m (the measurement was done at room temperature). The

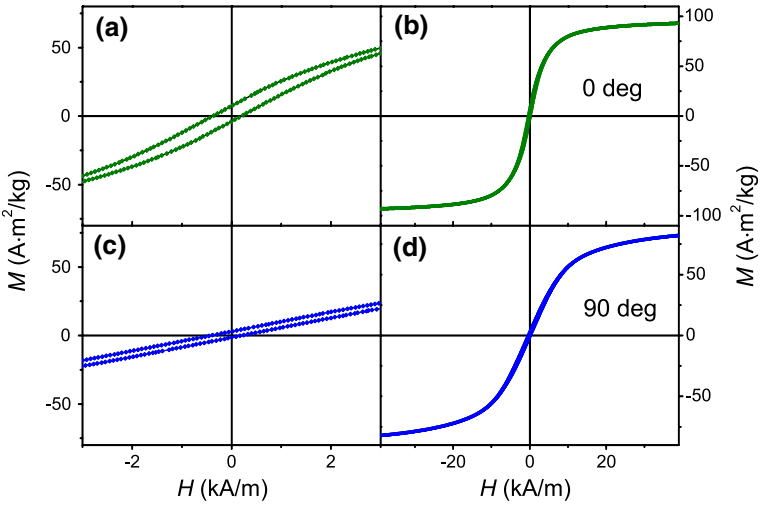

Fig. 6 Magnetic hysteresis loops at room temperature of $Ni_{45}Co_5Mn_{35.5}In_{14.5}$ for two different orientations of the sample

field cooling procedure was not applied during the measurement, but it is not a necessary condition for EB observation. Wang et al. [29] report about exchange bias effect in Ni-Mn-In bulk sample after zero field cooling from an unmagnetized state. In Fig. 7, dependence of bias field H_e on the angle φ between the external magnetic field and the longest edge of the specimen is presented. The shape of the line is different from the dependence observed for AFM and FM layers measured experimentally in [30] or calculated theoretically in [31], since the change of the H_e sign is not observed in our sample. This behavior can be related to the more complicated structure of $Ni_{45}Co_5Mn_{35.5}In_{14.5}$, where no planar FM and AFM layers are detected. The explanation of the observed $H_e(\varphi)$ dependence needs further research.

Cyclic EMR experiments based on repetition of measurements for a given orientation of the sample (fixed angle φ between the vector **B** and the symmetry axis of the specimen) were performed. The collected EMR signals for subsequent n measurement in the cycle allow determining the integral intensity I_{int} for each n. The dependence $I_{\text{int}}(n)$ presented in Fig. 8 indicates a decrease of intensity as the number n increases. Similar behavior of the EMR spectra was observed by Parekh [32], and was assigned to "training effect" [33]. This could also be an the explanation of the observed phenomenon for our sample.

4 Conclusion

The magnetic properties of Ni-Co-Mn-In have been investigated. VSM reveals a second-order phase transition from the PM to the FM state. The Curie temperature determined by the EMR method is in good agreement with T_C estimated by the VSM method. The upward deviation of the inverse integral intensity below T^* and the existence of the FMR line at the PM region can prove the coexistence of the magnetic phases in the sample. The additional phase is not observed in VSM results,

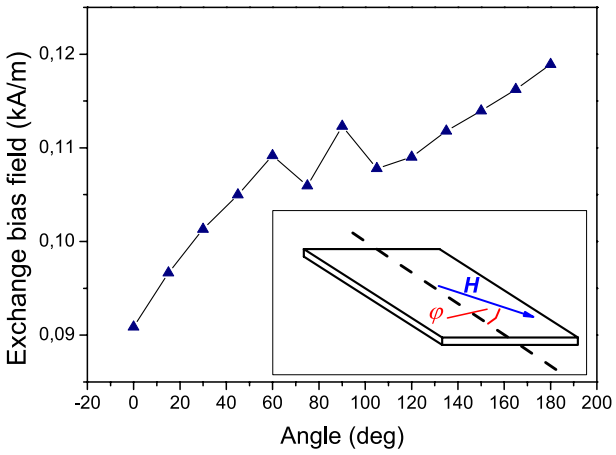

Fig. 7 Exchange bias field versus angle φ of $Ni_{45}Co_5Mn_{35.5}In_{14.5}$ ribbon at room temperature. Inset shows the experiment setup

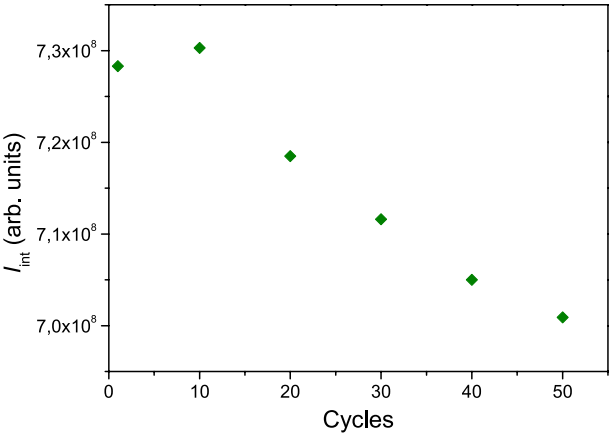

Fig. 8 Integrated intensity of EMR signal of the $Ni_{45}Co_5Mn_{35.5}In_{14.5}$ versus cycles

which underlines the importance of the EMR method in the study of magnetic properties. Spontaneous exchange bias effect observed at room temperature additionally confirms the existence of different magnetic phases in the sample.

References

1. X. Moya, L. Mañosa, A. Planes, T. Krenke, M. Acet, E.F. Wassermann, Mater. Sci. Eng., A **438-440**(SPEC. ISS.), 911 (2006). https://doi.org/10.1016/j.msea.2006.02.053
2. L. Chen, F.X. Hu, J. Wang, J. Shen, J.R. Sun, B.G. Shen, J.H. Yin, L.Q. Pan, Q.Z. Huang, J. Appl. Phys. **109**(7), 07A939 (2011). https://doi.org/10.1063/1.3565189
3. J.H. Chen, N.M. Bruno, I. Karaman, Y. Huang, J. Li, J.H. Ross, J. Appl. Phys. **116**(20) (2014). https://doi.org/10.1063/1.4902527
4. Y. Feng, J.H. Sui, Z.Y. Gao, G.F. Dong, W. Cai, J. Alloys Compd. **476**(1–2), 935 (2009). https://doi.org/10.1016/j.jallcom.2008.09.149
5. Z.H. Liu, H. Liu, X.X. Zhang, M. Zhang, X.F. Dai, H.N. Hu, J.L. Chen, G.H. Wu, Phys. Lett. A. **329**(3), 214 (2004). https://doi.org/10.1016/j.physleta.2004.06.088
6. X.G. Zhao, C.C. Hsieh, J.H. Lai, X.J. Cheng, W.C. Chang, W.B. Cui, W. Liu, Z.D. Zhang, Scr. Mater. **63**(2), 250 (2010). https://doi.org/10.1016/j.scriptamat.2010.03.067
7. G.H. Yu, Y.L. Xu, Z.H. Liu, H.M. Qiu, Z.Y. Zhu, X.-P. Huang, L.-Q. Pan, Rare Met. **34**, 527 (2015). https://doi.org/10.1007/s12598-015-0534-1
8. C. Jing, J. Chen, Z. Li, Y. Qiao, B. Kang, S. Cao, J. Zhang, J. Alloys Compd. **475**(1–2), 1 (2009). https://doi.org/10.1016/j.jallcom.2008.07.012
9. Y. Chen, J. Lin, I. Titov, A. Granovsky, J. Magn. Magn. Mater. **407**, 365 (2016). https://doi.org/10.1016/j.jmmm.2016.01.079
10. W.H. Meiklejohn, C.P. Bean, Phys. Rev. **102**(5), 1413 (1956). https://doi.org/10.1103/PhysRev.102.1413
11. P.A. Bhobe, K.R. Priolkar, A.K. Nigam, J. Phys. D: Appl. Phys **41**(23), 235006 (2008). https://doi.org/10.1088/0022-3727/41/23/235006

12. E. Sasioglu, L.M. Sandratskii, P. Bruno, Phys. Rev. B **70**(2), 1 (2004). https://doi.org/10.1103/PhysRevB.70.024427
13. J. Nogués, I.K. Schuller, J. Magn. Magn. Mater. **192**(2), 203 (1999). https://doi.org/10.1016/S0304-8853(98)00266-2
14. J. Nogués, J. Sort, V. Langlais, V. Skumryev, S. Suriñach, J.S. Muñoz, M.D. Baró, Phys. Rep. **422**, 65 (2005). https://doi.org/10.1016/j.physrep.2005.08.004
15. W. Maziarz, Solid State Phenomena **186**, 251 (2012). https://doi.org/10.4028/www.scientific.net/SSP.186.251
16. J. Deisenhofer, D. Braak, H.A. Krug von Nidda, J. Hemberger, R.M. Eremina, V.A. Ivanshin, A.M. Balbashov, G. Jug, A. Loidl, T. Kimura, Y. Tokura, Phys. Rev. Lett. **95**, 257202 (2005). https://doi.org/10.1103/PhysRevLett.95.257202
17. S.K. Misra, S.I. Andronenko, S. Asthana, D. Bahadur, J. Magn. Magn. Mater. **322**(19), 2902 (2010). https://doi.org/10.1016/j.jmmm.2010.05.003
18. S.I. Andronenko, A.A. Rodionov, A.V. Fedorova, S.K. Misra, J. Magn. Magn. Mater. **326**, 151 (2013). https://doi.org/10.1016/j.jmmm.2012.08.017
19. C. Autret-Lambert, M. Gervais, S. Roger, F. Gervais, M. Lethiecq, N. Raimboux, P. Simon, Solid State Sci. **71**, 139 (2017). https://doi.org/10.1016/j.solidstatesciences.2017.06.017
20. F.J. Dyson, Phys. Rev. **98**, 349–359 (1955). https://doi.org/10.1103/PhysRev.98.349
21. V.A. Ivanshin, J. Deisenhofer, H.A. Krug von Nidda, A. Loidl, A.A. Mukhin, A.M. Balbashov, M.V. Eremin, Phys. Rev. B **61**(23), 6213–6219 (2000). https://doi.org/10.1103/PhysRevB.61.6213
22. R.B. Griffiths, Phys. Rev. Lett. **23**, 17 (1969). https://doi.org/10.1103/PhysRevLett.23.17
23. S.N. Kaul, V. Siruguri, J. Phys. Condens. Matter **4**, 505 (1992). https://doi.org/10.1088/0953-8984/4/2/018
24. J.I. Prez-Landazbal, V. Recarte, V. Snchez-Alarcos, C. Gmez-Polo, E. Cesari, Appl. Phys. Lett. **102**(10), 101908 (2013). https://doi.org/10.1063/1.4795716
25. S. Zhou, L. Shi, H. Yang, J. Zhao, Appl. Phys. Lett. **91**(17), 6 (2007). https://doi.org/10.1063/1.2801694
26. A. Aharoni, J. Appl. Phys. **83**(6), 3432 (1998). https://doi.org/10.1063/1.367113
27. A.K. Pathak, M. Khan, B.R. Gautam, S. Stadler, I. Dubenko, N. Ali, J. Magn. Magn. Mater. **321**(8), 963 (2009). https://doi.org/10.1016/j.jmmm.2008.03.008
28. P. Czaja, M. Fitta, J. Przewoźnik, W. Maziarz, J. Morgiel, T. Czeppe, E. Cesari, Acta Mater. **103**, 30 (2016). https://doi.org/10.1016/j.actamat.2015.10.001
29. B.M. Wang, Y. Liu, P. Ren, B. Xia, K.B. Ruan, J.B. Yi, J. Ding, X.G. Li, L. Wang, Phys. Rev. Lett. **106**(7), 077203 (2011). https://doi.org/10.1103/PhysRevLett.106.077203
30. B.B. Singh, S. Chaudhary, J. Magn. Magn. Mater. **385**, 166 (2015). https://doi.org/10.1016/j.jmmm.2015.03.004
31. J. Geshev, L.G. Pereira, J.E. Schmidt, Phys. Rev. B **64**(18), 184411 (2001). https://doi.org/10.1103/PhysRevB.64.184411
32. K. Parekh, R.V. Upadhyay, J. Magn. Reson. **225**, 46 (2012). https://doi.org/10.1016/j.jmr.2012.10.001
33. S. Giri, M. Patra, S. Majumdar, J. Phys. Condens. Matter **23**, 073201 (2011). https://doi.org/10.1088/0953-8984/23/7/073201